

Cross sections for $\gamma\gamma \rightarrow \mu^+\mu^-$ and $\gamma\gamma \rightarrow e^+e^-$

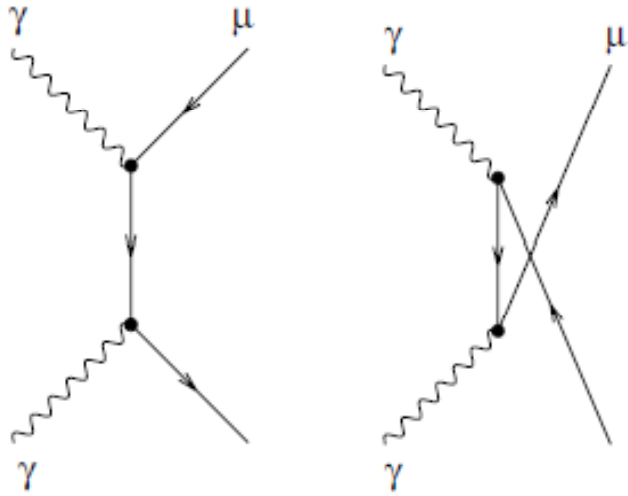


Figure 2.2: Two-photon subprocess. Shown are the t-channel (right) and the u-channel (left) contribution.

Neglecting the muon mass:
Cross section peaks in forward and
backward directions

$$\frac{d\sigma}{dt} = \frac{2\pi\alpha^2}{s} \left(\frac{u}{t} + \frac{t}{u} \right)$$

Bjorken and Drell for pair annihilation, μ^- is at rest in the lab frame :

$$\frac{d\sigma(\mu^+ \mu^- \rightarrow \gamma_1 \gamma_2)}{d\Omega_{LAB-\gamma_1}} = \sum_{\varepsilon_1 \varepsilon_2} \frac{\alpha^2 (m + E_+)}{8p_+ (m + E_+ - p_+ \cos \theta)^2} \left[\frac{E_+ - p_+ \cos \theta}{m} + \frac{m}{E_+ - p_+ \cos \theta} + 2 - 4(\vec{\varepsilon}_1 \cdot \vec{\varepsilon}_2)^2 \right]$$

Boost into the CM frame:

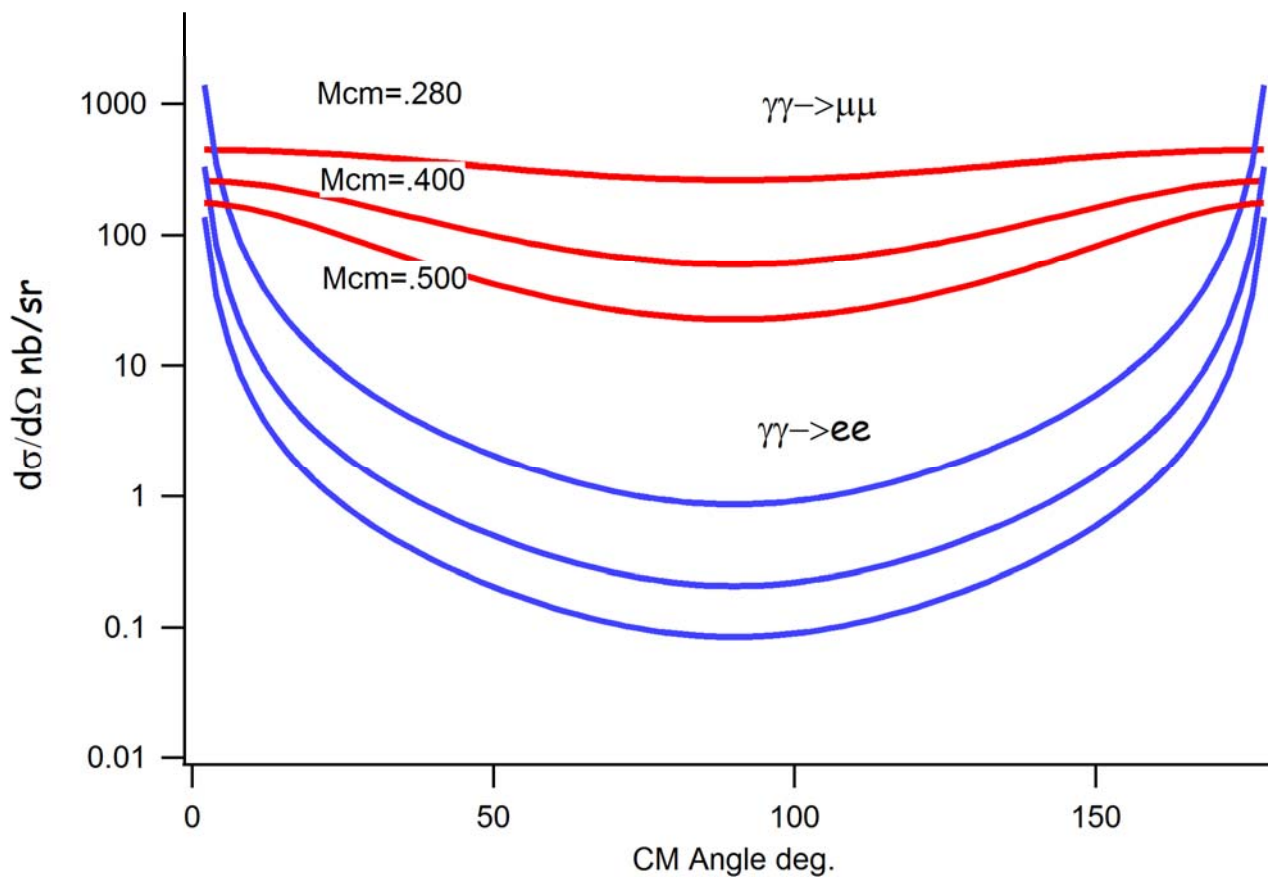
$$\frac{d\sigma(\mu^+ \mu^- \rightarrow \gamma_1 \gamma_2)}{d\Omega_{CM}} = \frac{d\Omega_{LAB-\gamma_1}}{d\Omega_{CM}} \cdot \frac{d\sigma(\mu^+ \mu^- \rightarrow \gamma_1 \gamma_2)}{d\Omega_{LAB-\gamma_1}}$$

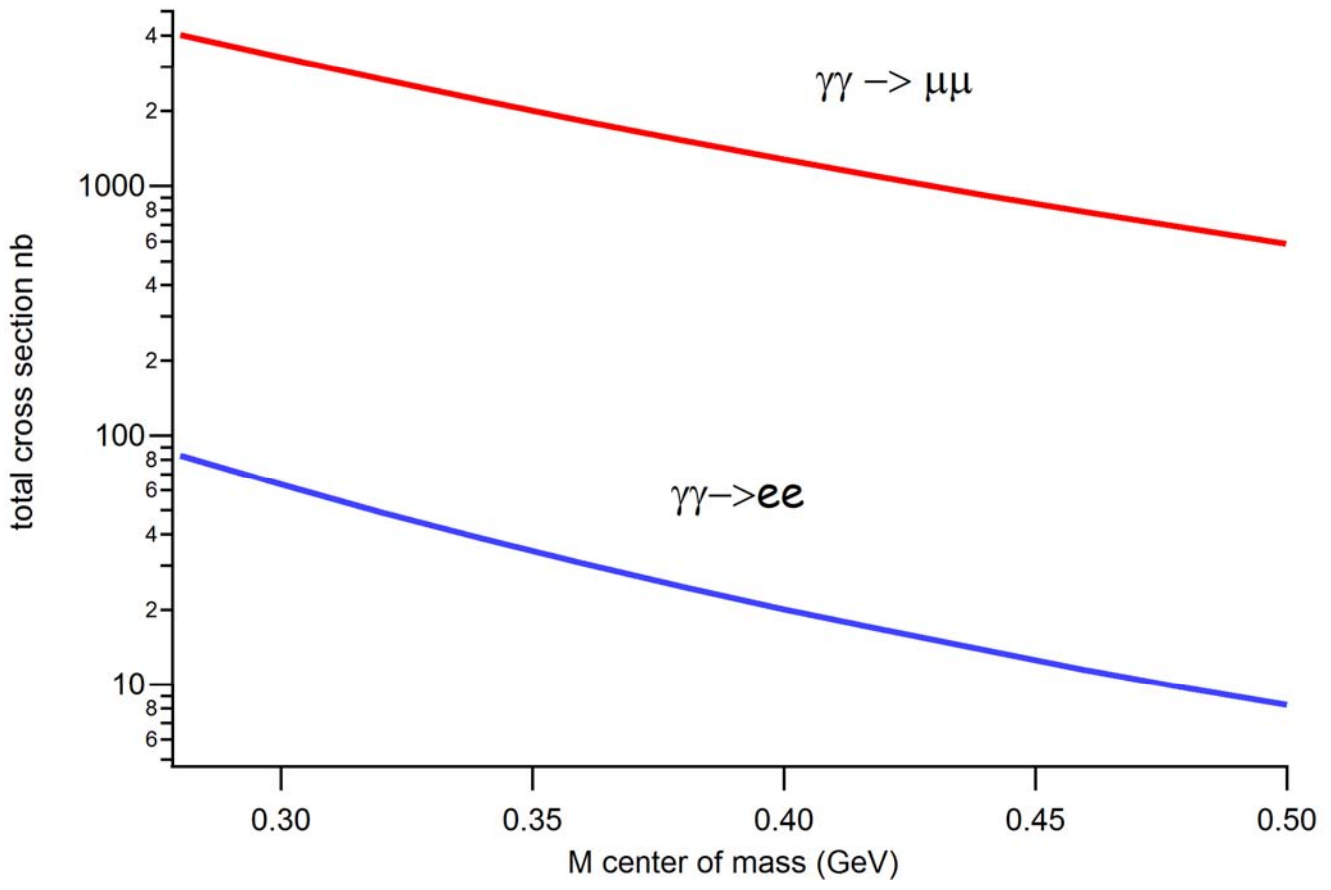
Detailed balance:

$$\frac{d\sigma(\mu^+ \mu^- \rightarrow \gamma_1 \gamma_2)}{d\Omega_{CM}} = \frac{1}{2} |M_{fi}|^2 \frac{(2)^2}{v_i v_f} P_\gamma^2$$

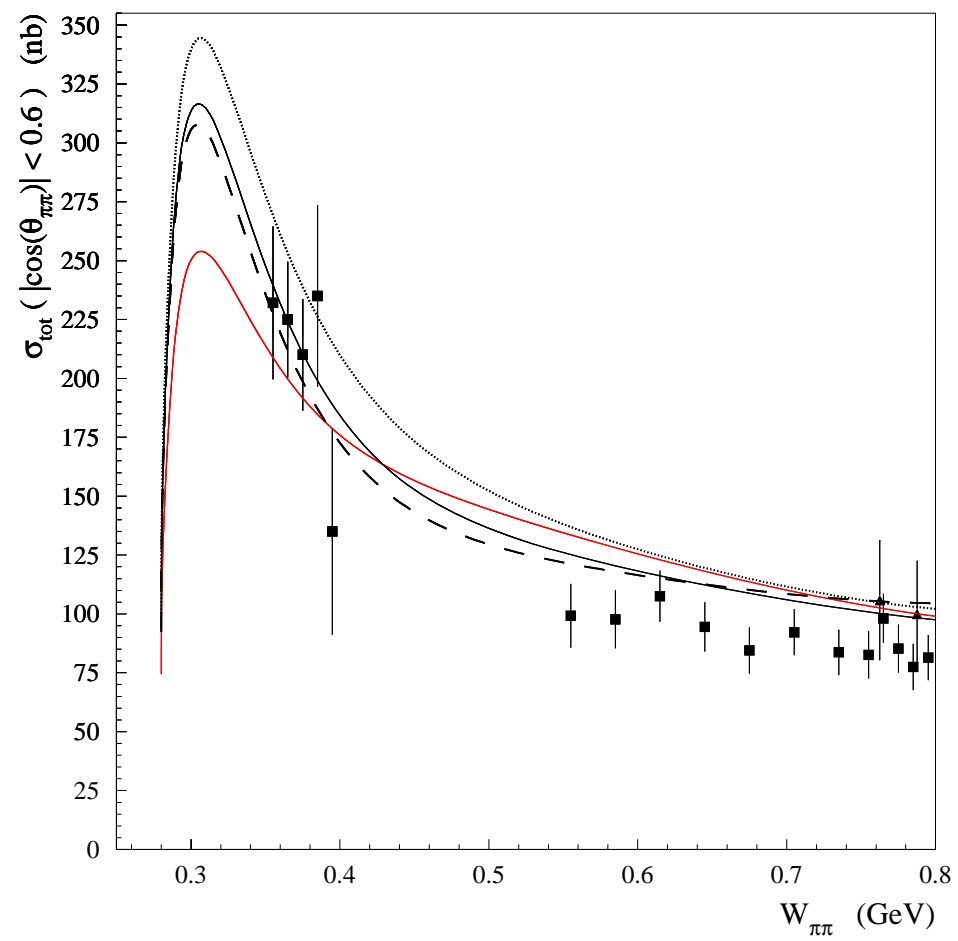
$$\frac{d\sigma(\gamma\gamma \rightarrow \mu^+ \mu^-)}{d\Omega_{CM}} = |M_{fi}|^2 \frac{(2)^2}{v_f v_i} P_\mu^2$$

$$\frac{d\sigma(\gamma\gamma \rightarrow \mu^+ \mu^-)}{d\Omega_{CM}} = 2 \frac{d\sigma(\mu^+ \mu^- \rightarrow \gamma_1 \gamma_2)}{d\Omega_{CM}} \left(\frac{P_\mu}{P_\gamma} \right)^2$$





$\gamma + \gamma \rightarrow \pi^+ + \pi^-$



Primakoff cross sections:

$$\frac{d^2\sigma(\gamma A \rightarrow \mu^+ \mu^- A)}{d\Omega dM} = \frac{2\alpha Z^2}{\pi^2} \frac{E_\gamma^4 \beta^2}{M} \frac{\sin^2 \theta}{Q^4} \sigma(\gamma\gamma \rightarrow \mu^+ \mu^-)$$

- Find cross sections and acceptance for e^+e^- and $\mu^+\mu^-$ events
- Model the size of muon detector

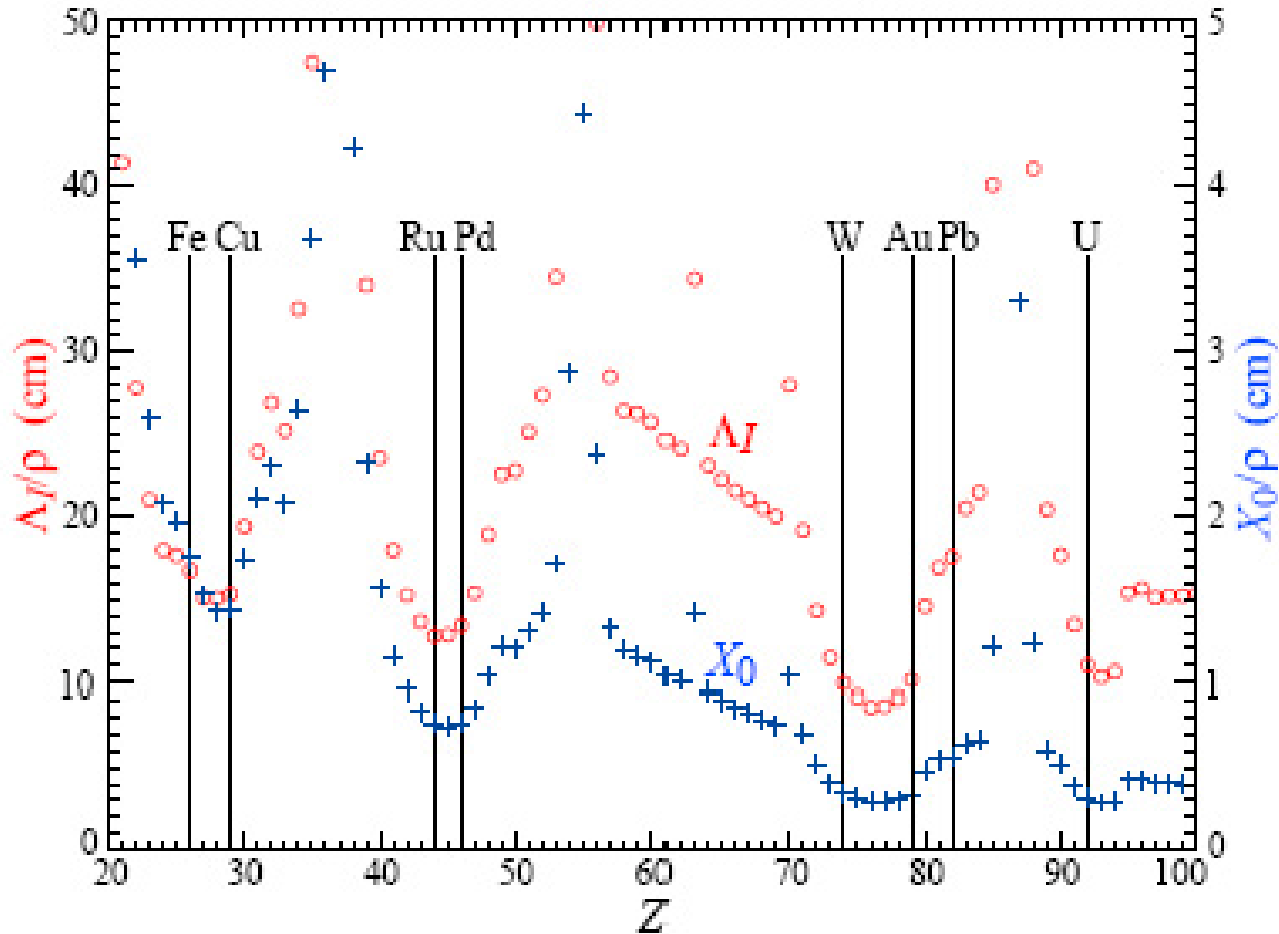


Figure 28.21: Nuclear interaction length λ_I/ρ (circles) and radiation length X_0/ρ (+’s) in cm for the chemical elements with $Z > 20$ and $\lambda_I < 50$ cm.

In all cases there is a premium on small λ_I/ρ and X_0/ρ (both with units of length). These quantities are shown for $Z > 20$ for the chemical elements in Fig. 28.21. For the hadronic case, metallic absorbers in the W–Au region are best, followed by U. The Ru–Pd region elements are rare and expensive. Lead is a bad choice. Given cost considerations, Fe and Cu might be appropriate choices. For EM calorimeters high Z is preferred, and lead is not a bad choice.

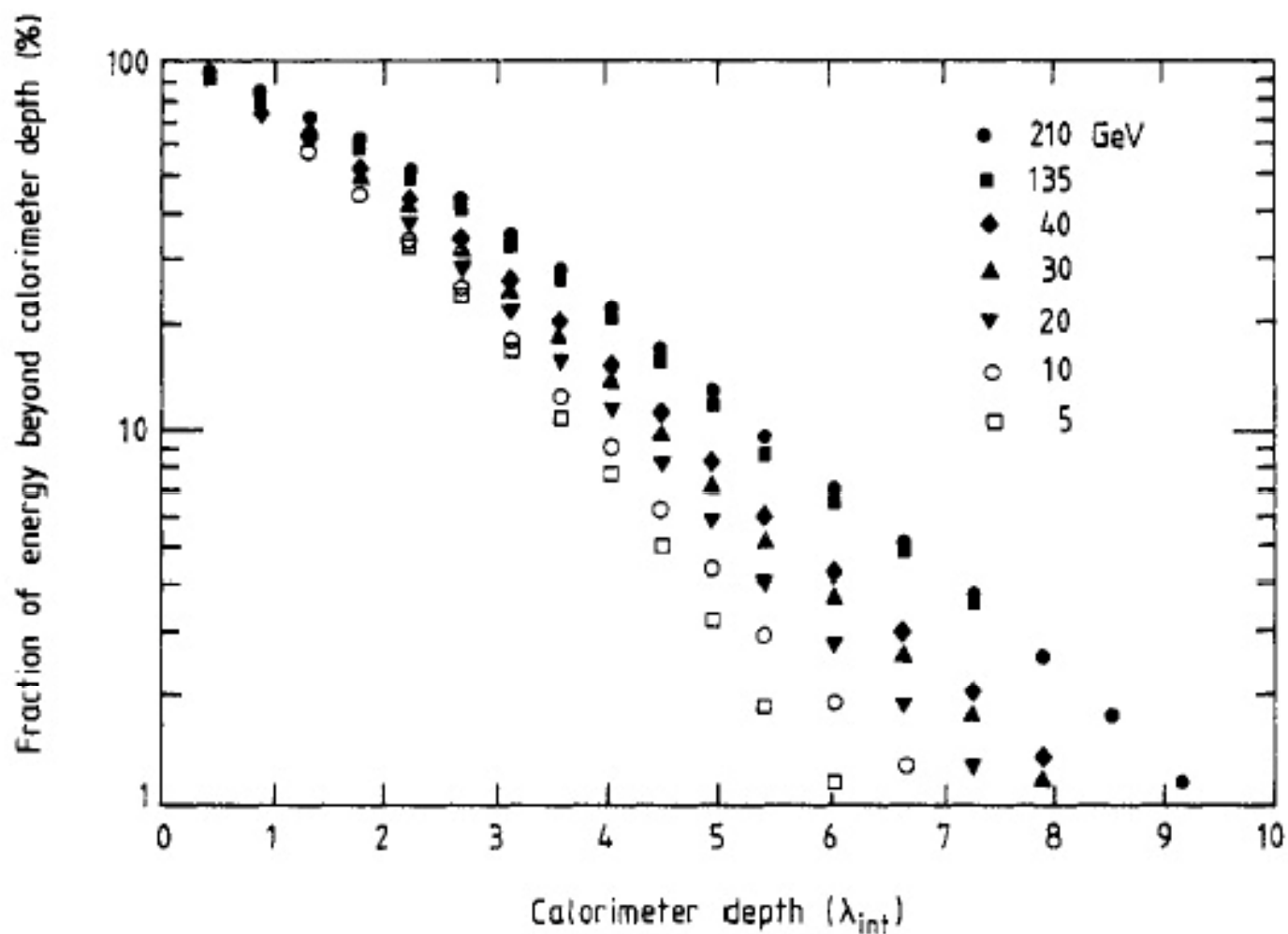
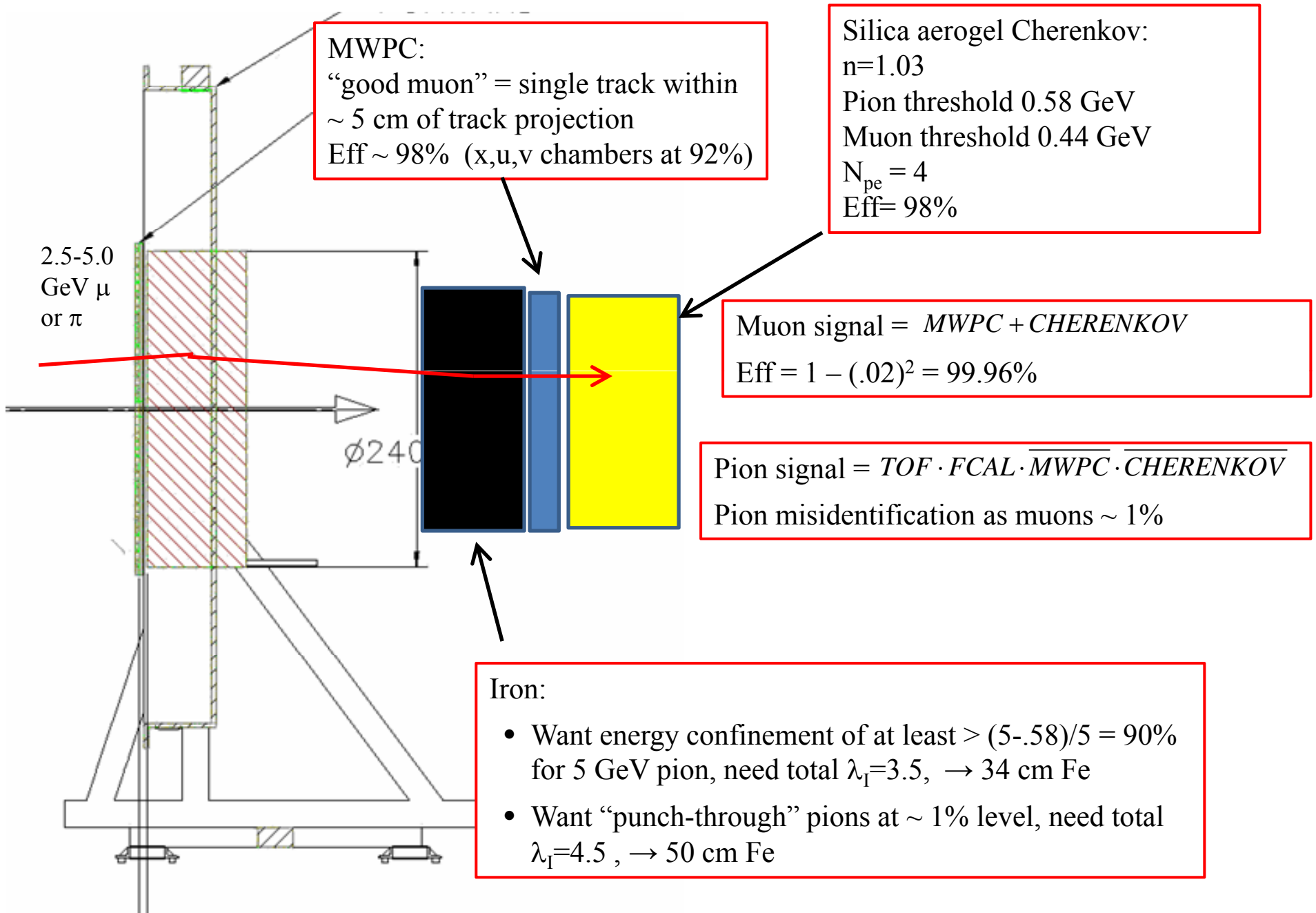


Figure 7. The leakage as a function of the detector depth, for pions of 5–210 GeV, measured in a uranium/plastic-scintillator calorimeter. Data from Catanesi *et al* (1987).



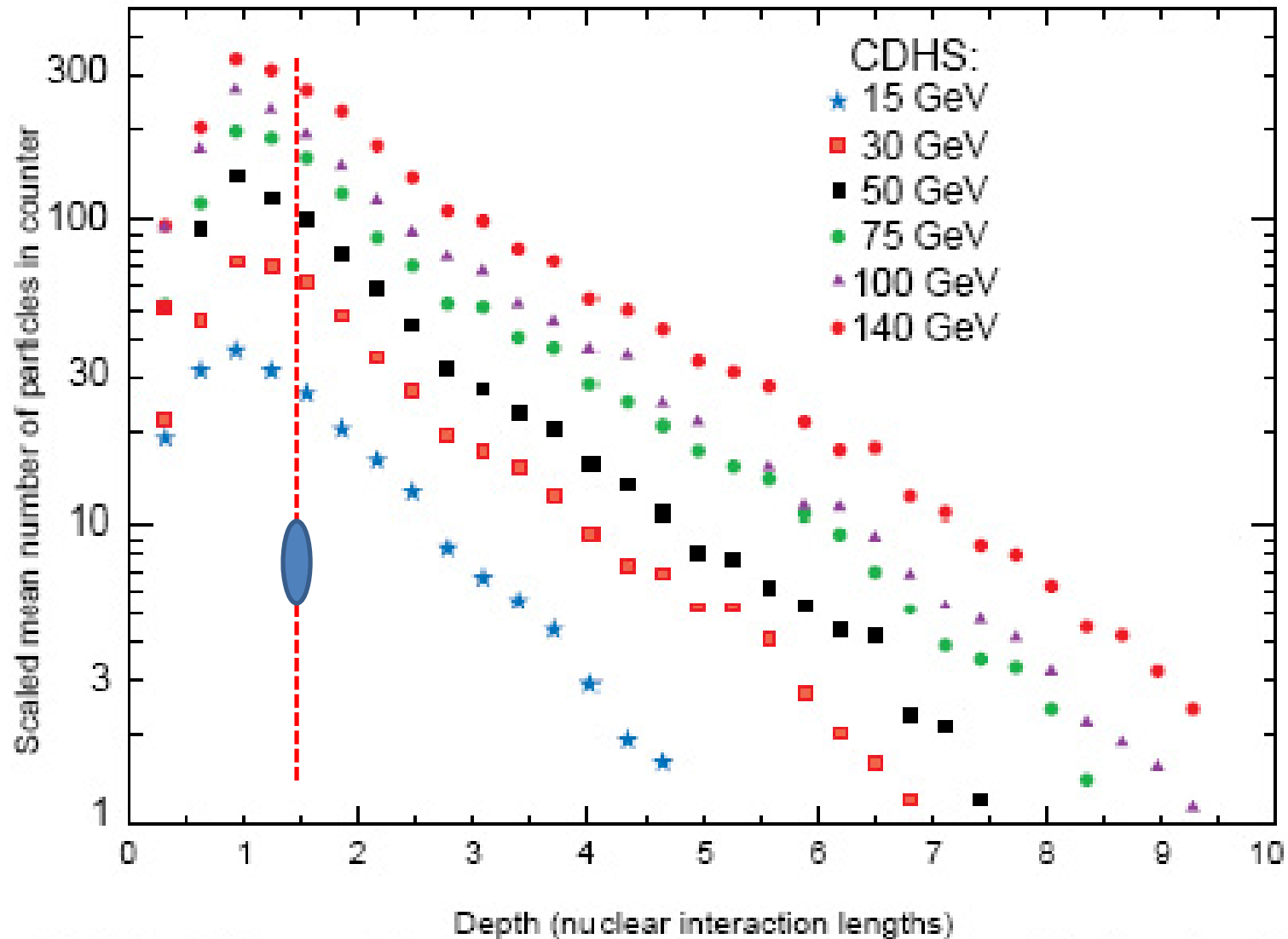
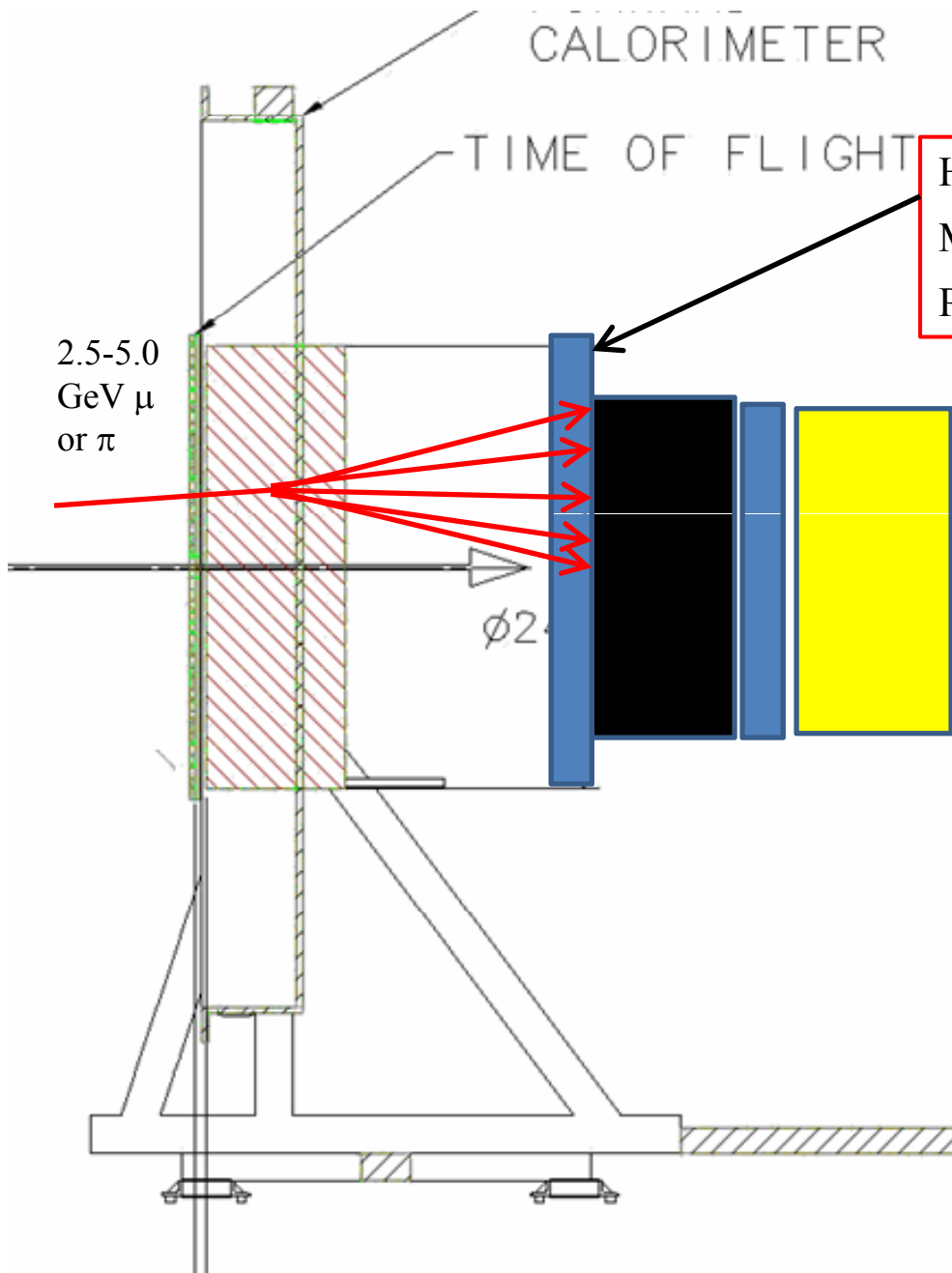


Figure 28.23: Mean profiles of π^+ (mostly) induced cascades in the CDHS neutrino detector [143]. See full-color version on color pages at end of book.



How efficient is $TOF \cdot FCAL$
 MWPC as pion detector?
 Pion signal = $TOF \cdot (FCAL + MWPC_1) \cdot \overline{MWPC_2} \cdot \overline{C}$

FCAL efficiency for pions ~ 95%?
 MPWPC efficiency for pions 98%
 FCAL + MWPC efficiency 99.9%